Melone's Concept Revisited: 3D Quantification of Fragment Displacement

Teun Teunis[1] Niels H. Bosma[1] Bart Lubberts[1] Dirk P. Ter Meulen[1] David Ring[2]

[1] Orthopaedic Hand and Upper Extremity Service, Massachusetts General Hospital, Harvard Medical School, Boston, Massachusetts, United States
[2] Dell Medical School, The University of Austin at Texas, Texas, United States

Address for correspondence David Ring, MD, PhD, Dell Medical School, The University of Austin at Texas, Texas, United States (e-mail: dring@mgh.harvard.edu).

J Hand Microsurg 2016;8:27–33.

Abstract

We applied quantitative 3D computed tomography to 50 complete articular AO type C fractures of the distal radius and tested the null hypothesis that fracture fragments can be divided according to Melone's concept (radial styloid and volar and dorsal lunate facet fragments) and that each fragment has similar (1) displacement and (2) articular surface area. Thirty-eight fractures fit the Melone distribution of fragments. Radial styloid fragments were most displaced, and volar lunate fragments were least displaced. Volar lunate fragments had the largest articular surface area. While these findings confirm Melone's concepts, the finding that volar lunate fragments are relatively large and dorsal lunate fragments relatively small suggests that alignment of the volar lunate fragment with the radial styloid may be the key element of treatment and the dorsal lunate fragment may not routinely benefit from specific reduction and fixation.

Keywords
- computed tomography
- distal radius
- fractures
- morphology
- quantitative

Introduction

Approximately half of all distal radius fractures are intra-articular, and the majority (~80%) are complete articular fractures (AO type C).[1,2] Melone emphasized the importance of the lunate facet in complete articular type C fractures based on wisdom rather than measurements and data. In particular, he emphasized the importance of a coronal plane fracture line creating separate volar and dorsal lunate facet fragments. An unstable malrotated volar lunate facet fragment was felt to be irreducible with manipulation alone, and open reduction and plate fixation was recommended.[3–7] Medoff divided type C articular fracture fragments into radial column, ulnar corner, dorsal wall, volar rim, and free intra-articular fragments. These classifications are useful conceptually for characterizing the fracture patterns, defining important fracture elements, and directing effective management of each fracture, but they are conceptual and merit confirmation with direct assessment of fracture patterns and measurements.

Quantitative 3D computed tomography (Q3DCT) measures the number, 3D displacement, and articular surface area of fracture fragments.[8,9] These quantitative measurements might provide a more detailed understanding of fracture morphology, refine our concepts about fracture patterns and fragment morphology, and help plan treatment.[9] We used these methods to measure fracture fragments of complete intra-articular distal radius fractures to determine if Melone's concepts were accurate and to determine the relative size of the various fragments.

We applied the technique of Q3DCT to complete articular (AO type C) fractures of the distal radius and tested the null hypothesis that AO type C fracture fragments can be divided according to Melone's concepts and that they have similar (1) displacement and (2) articular surface area. Secondarily, we compared gap measured on radiographs and CT scans with Q3DCT gap surface area.

Materials and Methods

Patient Selection

After approval by our institutional review board, we retrospectively included 69 consecutive patients with intra-

received
May 18, 2015
accepted after revision
March 9, 2016

DOI http://dx.doi.org/10.1055/s-0036-1581125.
ISSN 0974-3227.

articular distal radius fractures who underwent CT scanning at our institution. Patients were treated between January 5, 2009, and September 24, 2012. We excluded 15 patients with insufficient quality scans (slice thickness $>$ 1.25 mm) and 4 patients with AO type B fractures. Fifty patients with AO type C fractures were included in our final analysis. Two authors individually classified the fractures based on 3D models. In case of a discrepancy, D. R. opinion was definitive. Median time to CT scan after injury was 1 day (interquartile range [IQR], 0–6). All wrists were splinted in the emergency department. In total, 40 fractures (89%) were reduced prior to CT scanning (177 fracture fragments), 5 were not reduced (19 fragments), and the reduction status could not be determined for 5 fractures (23 fragments). We found no difference in 3D displacement measured by Q3DCT based on reduction status (unreduced 2.8 mm [IQR, 1.2–4.4] vs. reduced 3.4 mm [IQR, 1.7–6.2] vs. unknown 6.1 mm [IQR, 3.4–8.9]; $p = 0.20$).

3D Modeling

CT scans were saved as Digital Imaging and Communications in Medicine (DICOM) files and were then loaded into 3D Slicer (version 4.2.0; Boston, Massachusetts, United States). A threshold of 250 Hounsfield units was used to identify fracture fragments; at this threshold even small fragments can be identified, but the distortion from surrounding soft tissue is minimal. Subsequently, all 3D models were exported into Rhinoceros (Rhinoceros 5.0, McNeel; Seattle, Washington, United States) for further analysis. We determined the number of articular fragments, their displacement, articular surface area, and articular fracture lines.

The position of the 3D models was standardized using the x-, y-, and z-axes in Rhinoceros; the medullary canal was used to define proximal and distal (z-axis), and the volar side was used to define radial and ulnar (x-axis) and volar and dorsal (y-axis). All 28 3D models of left-sided radii were mirrored to make the orientation match that of the right-sided radii (see http://youtu.be/M0niRAoZ2xw for explanatory video).[10]

Fracture Fragments

Our total of 50 fractures created 180 articular fragments. The majority were classified (by author consensus) as AO type C3 ($n = 41$). Six were classified as type C2 and three as type C1 (►**Table 1**). C3 fractures that could not be classified by Melone and AO type C1 and C2 are grouped and reported separately. All such fractures consisted of one large fragment and one or more smaller fragments, except for one AO C3.3 fracture that was excluded from the analysis.

Displacement

First, we determined the coordinates for the center of each fracture fragment in 3D space. The fracture was then reassembled using an unfractured distal radius as an overlay template to approximate shape of the native preinjury anatomy. We defined displacement as the difference between the coordinates of the fracture fragment in this new position and the original coordinates (►**Fig. 1**). The overlay template was positioned at the beginning of the study and then remained in this position throughout the study. The template size was adjusted to match the 3D fracture model, without changing its position. Using the medullary canal of the radial diaphysis, we arranged the axes so that displacement on the z-axis represented proximal–distal displacement (loss of height), the x-axis radial–ulnar displacement, and the y-axis volar–dorsal displacement. Overall multidirectional (3D) displacement was defined as combined x-, y-, and z-axis displacement:

$$\text{3D displacement (mm)} = (\sqrt{(\Delta x^2 + \Delta y^2 + \Delta z^2)}$$

In case of a split radial styloid, medial volar, or dorsal fragment, the average displacement of the fragments was calculated.

Articular Surface and Gap Deformity

Articular surface area was determined by outlining the edges of the articular surface area of each fragment. Subsequently, the surface area, following the contours of the outlined area, was calculated. We compared gap deformity measured on radiographs and in our 3D models. First, we retrieved all radiographs made closest to the time of CT scanning and measured absolute gap deformity on lateral and posterior–anterior radiographs as previously described[11] using Onis (2.5 Free Edition, DigitalCore, Tokyo). Second, to measure gap deformity between fracture fragments in our 3D models, we outlined the edges of the gap at the level of the articular surface. Subsequently, we measured the size of the gap perpendicular to the x-axis (radioulnar, similar to posterior–anterior radiographs) and y-axis (volar–dorsal; lateral radiographs) to establish absolute gap deformity. We also calculated the surface area of the outlined gap (►**Fig. 2**).

Fracture Lines

To allow for analysis of fracture lines, we created similar-sized radii by resizing all the fractured radii to match the preinjury template's size. Subsequently, the carpal articular surface was outlined and each patient's fracture lines were plotted into this outline. Line coordinates were exported to Wolfram Mathematica (Wolfram Mathematica 9.0, Wolfram Research, Champaign, Illinois, United States). We created a heat map by plotting (1) fractures lines that fit the Melone classification and (2) other type C fractures, following light's visible color spectrum: purple indicates a low density and red a high density of fracture lines. The circumference of the model was divided into barren zones and zones with capsular and ligamentous attachment as described by previous studies.[12,13] We counted the number of fracture line that exited through either type of zone.

Measurement Reliability

Measurement variability can arise in (1) 3D model positioning, (2) fracture reduction, and (3) surface area outlining (see the sections "Displacement" and "Articular Surface and Gap Deformity" in the Materials and Methods section). The same two investigators both independently positioned and measured a set of 10 randomly selected unreduced fracture models to assess the reliability of measuring area and 3D displacement.

Table 1 Baseline fracture characteristics

AO fracture type	Number			
C1	3			
C2	6			
C3	41			
C3 Melone fragments	**Intact**	**Split**	**Double split**	**Triple split**
Radial styloid	20	14	3	1
Volar medial	34	4		
Dorsal medial	29	8	1	
C3 Fractures that not fit Melone	**Number**			
High coronal/die punch	2			
AO type C3.3	1			
Gap deformity[a]	**Radiographs**		**Computed tomography**	***p*-Value**
Volar–dorsal (y-axis)	3.8 (0–7.0) mm		11 (7.7–17) mm	<0.001
Radioulnar (x-axis)	3.1 (0–5.4) mm		16 (8.2–25) mm	<0.001
Gap surface area[a]	40 (21–95) mm^2			
Fracture lines	**Number (%)**			
Through soft tissue	72 (38%)			
Through barren bone	118 (62%)			

Note: $n = 50$.
[a]Median (interquartile range).

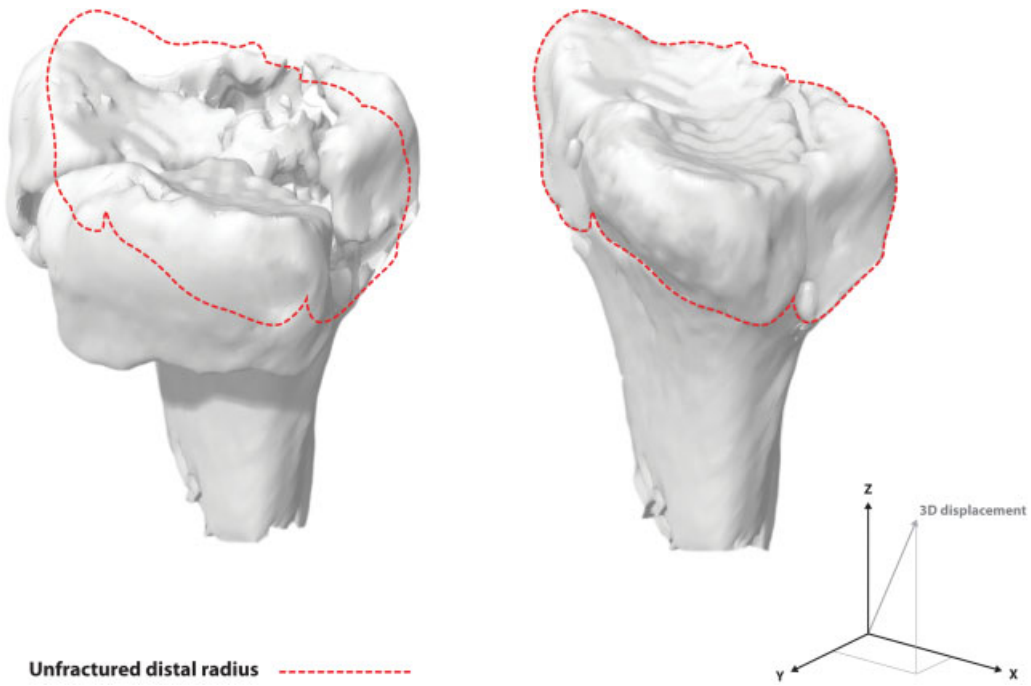

Fig. 1 Unreduced and reduced distal radius fracture model. A fractured radius is shown on the left; the fractured radial diaphysis is already positioned within that of the template (not shown). The fracture fragments are reduced within the unfractured template, shown on the right. The outline of the template's metaphysis is represented by the red dotted line. In the right lower corner, the template's orientation is shown: z-axis represents proximal–distal displacement (loss of height), the x-axis radial–ulnar displacement, and the y-axis volar–dorsal displacement. Overall, multidirectional (3D) displacement is the vector of those axes.

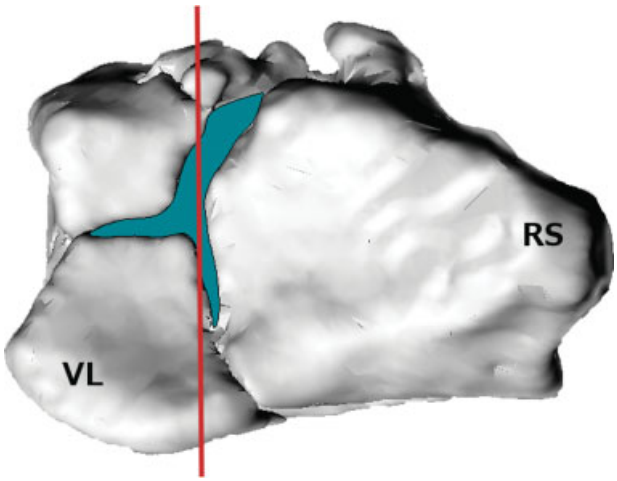

Fig. 2 Outlined area of gap deformity. The top view of the distal radius articular surface is shown. The red line indicates potential measured absolute gap on sagittal CT view, actually representing the split between the lunate facets and radial styloid. This would results in an overestimation of actual gap. Gap surface area is shown in green. RS, radial styloid; VL, volar lunate facet.

Statistics

Due to the mainly nongaussian distribution assessed by Shapiro–Wilk test, we calculated the median and IQR and used nonparametric testing. Values of p less than 0.05 were considered significant.

Interobserver agreement of the displacement and articular surface area by the same set of two independent observers was evaluated by an intraclass correlation coefficient through a two-way mixed effects model with absolute agreement. Absolute agreement in an intraclass correlation assesses how much each measurement performed per observer differs from the other observer. The intraclass correlation coefficient was 0.82 for 3D displacement (95% confidence interval [CI], 0.69–0.90), 0.91 for articular surface area (95% CI, 0.84–0.96), and 0.93 for gap surface (95% CI, 0.74–0.98), all $p < 0.001$. An intraclass correlation above 0.8 indicates a very high interobserver agreement.

As our sample size was limited by the available CT scans and resources, no power analysis was performed.

Results

Of the 41 C3 fractures, 38 (93%) fit the Melone distribution of fragments, but there were 3 exceptions: 1 fracture had a coronal fracture line, but intact sigmoid fossa (AO type C3.3),[2] and 2 had a high coronal/large die-punch fracture that extended more radial with no split in the large volar fragment (sequentially fracture 19, 24, and 29 in ►**Supplementary Fig. 1** available in the online version of this article). Of the 38 fractures that fit the Melone distribution of fragments, 20 fractures had a single radial styloid fragment and 18 were fragmented (one fracture line, $n = 14$; two fracture lines, $n = 3$; and three fracture lines, $n = 1$). A total of 34 volar medial fragments were single fragments, and 4 were split into two parts. Of the dorsal medial fragments, 29 were single fragments, 8 were split once, and 1 consisted of three parts (►**Table 1**). The majority (62% [118 of 190]) of the fractures lines exited through parts of the radius without ligament attachments (►**Table 1**). A heat map of the Melone fracture patterns shows a relatively intact volar medial fragment (purple) and a high concentration of fractures on the dorsal ridge of the lunate fossa (red) (►**Fig. 3**). A heat map of the other fractures indicates a high fracture line density entering the sigmoid fossa.

Among the fractures with typical Melone fragments—that is, a radial styloid and dorsal and volar lunate facet fragment—the radial styloid fragments were on average most displaced and volar medial fragments were least displaced (►**Table 1**).

Volar medial fragments had the largest articular surface area on average (39% [188 of 484 mm^2]) when compared with radial styloid (37% [178 of 484 mm^2]) and dorsal medial fragments (24% [118 of 484 mm^2]; $p < 0.001$) (►**Table 2**). Among type C fractures that did not have the typical Melone fragments, we found no difference in displacement between large and smaller fragments. As one would expect, larger

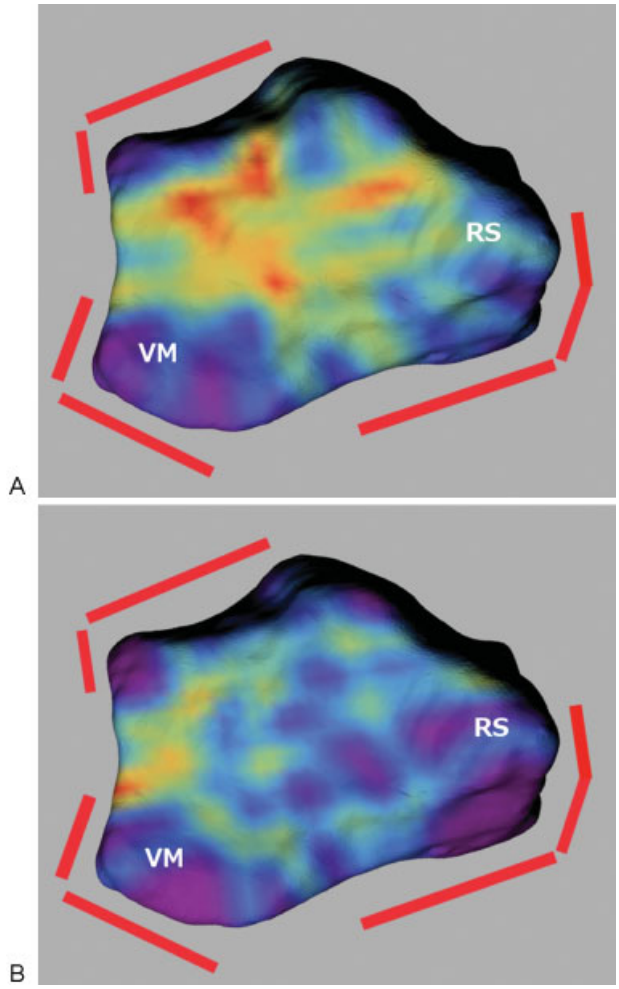

Fig. 3 Heat map of the density of all fracture lines. (**A**) Melone fractures. (**B**) Other type C fractures. Fracture line density follows light's visible color spectrum: purple indicates a low density (<0.5% of all fracture coordinates) and red a high density (>10% of all fracture coordinates) of fractures. Red lines indicate ligamentous attachments.[12,13] RS, radial styloid; VM, volar medial.

Table 2 Type C fractures of the distal radius: displacement and articular surface area

	Displacement of the centroid of the fracture fragment								Articular surface	*p*-Value	Percentage of total surface
	Proximal–distal displacement	*p*-Value	Radial–ulnar displacement	*p*-Value	Volar–dorsal displacement	*p*-Value	3D displacement	*p*-Value			
Fractures fitting Melone classification ($n = 38$)											
Radial styloid	2.1 (0.65–5.6)	0.042	2.8 (0.87–4.3)	<0.001	3.1 (1.4–7.4)	0.037	5.4 (2.8–10)	0.0014	149 (91–255)	<0.001	37% (178/484)
Volar medial	0.97 (0.22–1.9)		0.49 (0.03–1.5)		1.5 (0.3–2.9)		2.2 (1.2–4.6)		170 (136–225)		39% (188/484)
Dorsal medial	1.8 (0.87–3.4)		1.1 (0.32–2.7)		2.5 (0.86–4.7)		3.8 (1.9–6.9)		89 (54–188)		24% (118/484)
Other type C fractures ($n = 11$)											
Large fragment	1.7 (0.43–5.7)	0.36	0.55 (0–2.3)	0.72	2.5 (0.47–3.4)	0.72	6 (2.3–8)	0.41	274 (252–450)	<0.001	73% (320/439)
Smaller fragments	0.69 (0.34–2.4)		1 (0.03–2.5)		1.7 (0.01–4.4)		2.6 (1.2–5.9)		122 (54–141)		27% (119/439)

Note: Displacement in mm, surface in mm^2; n = number. Values are given as median (interquartile range) and surface area % as mean. One fracture remained unclassifiable (see **►Supplementary Figure 1** available in the online version of this article, fracture 19).

fragments had a larger articular surface (73% [320 of 439 mm^2] vs. 27% [119 of 439 mm^2]; $p < 0.001$).

Gap measured on posterior–anterior radiographs did not correlate with gap measured on frontal CT scans ($\rho = 0.26$; $p = 0.093$). However, Q3DCT gap surface area correlated with gap measured on both radiographs ($\rho = 0.45$; $p = 0.0023$) and CT scans ($\rho = 0.79$; $p < 0.001$). Lateral radiographic gap correlated somewhat with sagittal CT gap ($\rho = 0.37$; $p = 0.014$). Q3DCT gap surface area correlated highly with gap measured on both lateral radiographs ($\rho = 0.56$; $p < 0.001$) and sagittal CT scans ($\rho = 0.79$; $p < 0.001$) (►**Table 3**). The total combined area of the gap between fracture fragments averaged 40 mm^2 (range, 21–95 mm^2).

Discussion

We used Q3DCT to measure fracture patterns and fragment characteristics such as displacement in 3D, articular surface area, and total area of gaps between fragments. We confirmed Melone's concepts about fracture patterns and determined that the volar lunate fragment was much larger than the dorsal lunate fragment on average and the radial styloid fragment had the greatest average displacement.

This study has some limitations. First, the selection of fractures with CT scans and available in our sample may not be representative of the average type C fracture of the distal radius. Most of the fractures in our study featured limited displacement, which is probably representative of type C fractures in general. The amount of displacement is a factor used for surgical decision making. A study of more displaced fractures using Q3DCT might provide additional information. Second, our method does not allow measurement of fragment rotation, which is also an important aspect of fracture morphology.[14] Third, at least five fractures were not reduced prior to CT scanning, which affects the measured displacements and gaps.

Melone's concept is based on wisdom rather than measurements and data. The majority of fractures in our study fit the Melone distribution, confirming his influential ideas. However, the coronal split in the lunate facet is generally very dorsal, creating large volar lunate fragments (►**Fig. 3A**) that are more impacted than unstable by the ligamentous attachments, that is, least displaced (►**Table 2**). Our results also agree with a previous study indicating that fracture lines tend to occur between ligamentous attachments,[15] which may be the reason for the classic Melone grouping of fragments. Previous study found that most of the pressure with axial compression is transmitted across the intermediate column, for example, the lunate facet. This may be an explanation why articular comminution is found mainly at this level (dorsal and volar lunate facet). Similarly, our heat map shows the highest density of fracture lines at the intermediate column.[16]

Radial styloid fragments were on average more displaced, and volar lunate fragments were least displaced. Q3DCT measurements of fragment-specific 3D displacement might be useful in the study of treatment strategies and outcomes for complete articular fractures of the distal radius. Also, we

Table 3 Correlation of gap deformity measures on radiographs, CT, and Q3DCT

	Gap surface area	Radiographs
Frontal		
Gap surface area	–	–
Radiographs	0.45 (**0.0023**)	–
Computed tomography	0.79 (<**0.001**)	0.26 (0.093)
Lateral		
Gap surface area	–	–
Radiographs	0.56 (<**0.001**)	–
Computed tomography	0.79 (<**0.001**)	0.37 (**0.014**)

Note: Values are given as Spearman correlation (*p*-value). *p*-Values in bold indicate significance.

found that, on average, the volar lunate facet fragment is larger than the dorsal fragment. It is as if type C fractures exit the articular surface rather than the dorsal metaphysis as in a type A fractures. In other words, the dorsal lunate facet may often be part of the dorsal fragmentation typical of a dorsally displaced fracture. If the radiolunate ligaments are intact and the volar lunate facet fragment is reduced and secured, a relatively small, slightly displaced dorsal lunate fragment may not have much effect on function and may not merit an additional dorsal exposure—a hypothesis worth testing.

We encountered the following problem when measuring gap on CT. In a complete articular distal radius fracture with standard Melone configuration, there are two fracture lines in the carpal articular surface: (1) running from volar to dorsal with the radial styloid fragment on one side and the two volar and dorsal medial fragments on the other side; and (2) the fracture line between the volar and dorsal medial fragments. Gap measured in the sagittal plane evaluates the distance between the volar and dorsal medial fragments. However, when the image is almost exactly within the ventral to dorsal fracture line, this greatly overestimates the actual gap (see the red line in ►**Fig. 2**). The same occurs when assessing gap in frontal plane images: measuring gap within the fracture line between the dorsal and medial fragment can greatly overestimate this measure. To solve this, we propose Q3DCT surface area measurements for intra-articular gaps. By correlating clinical outcome to true surface of these gaps (as opposed to mere one-directional measures), we can gain further understanding of its role in predicting clinical outcome, as some literature suggests that conventional gap measures do not correlate with functional outcome.[17]

For the creation of 3D models and measurement of fracture characteristics, we used free and readily available software. Our results show measurement methods are reproducible between observers. A downside of Q3DCT is the labor intensiveness of 3D model creation, which increases with fracture complexity. Recently, software that uses a CT model from the intact opposite side to facilitate automatic reduction of fracture fragments is now available and might reduce the time per model, but this would require a CT scan of the opposite unfractured wrist.[18] Further development of this technique might further reduce interobserver variability, allowing Q3DCT to become a more widely used technique for fracture assessment.

Measurement of fracture fragments using software that allows sophisticated imaging and measurement of CT scans can improve our understanding of fractures. We studied a consecutive series of complete articular fractures and found limited displacement and large, easily managed volar lunate facets. The finding that volar lunate fragments are relatively large and dorsal ulnar fragments relatively small suggests that the highly influential theories and concepts of Melone may only apply to a smaller subset of type C fractures. Combining Q3DCT with patient-reported outcome and range of motion might help with the prediction of outcome after distal radius fractures and help guide treatment. Also, the difficulties in treatment of complex articular fractures relate to small volar lunate facets, complex fragmentation, central articular impaction, and more marked displacement. As Q3DCT can accurately quantify these aspects, this method can help to study areas of debate in the treatment of complete articular fractures. For example, (1) what size and displacement of dorsal lunate facet merits a separate dorsal exposure, reduction, and fixation? (2) Is there a subset of small volar lunate facet fragments that malrotate and hinder flexion (malangulation of the so-called teardrop on radiographs as described by Medoff)? (3) Is there a subset of small volar lunate facet fragments that can escape fixation and lead to subluxation of the carpus?

Note

All procedures performed in studies involving human participants were in accordance with the ethical standards of the institutional and/or national research committee and with the 1964 Declaration of Helsinki and its later amendments or comparable ethical standards.

Funding

T. T. received research grants from the Prince Bernhard Culture Fund & Kuitse Fund (less than US$10,000)

(Amsterdam, the Netherlands), Fundatie van de Vrijvrouwe van Renswoude te's-Gravenhage (less than US $10,000) (The Hague, the Netherlands).
D. R. certifies that he, or a member of his immediate family, has or may receive payments or benefits, during the study period from Wright Medical (less than US$10,000) (Memphis, Tennessee, United States), Skeletal Dynamics (less than US$10,000) (Miami, Florida, United States), Biomet (less than US$10,000) (Warsaw, Indiana, United States), AO North America (less than US$10,000) (Paoli, Pennsylvania, United States), and AO International (less than US$10,000) (Dubendorf, Switzerland).
All other authors have nothing to disclose.

References

1 McQueen MM, Jupiter JB. Musculoskeletal Trauma Series: Radius and Ulna. Oxford: Butterworth-Heinemann; 1999
2 Müller ME. The Comprehensive Classification of Fractures of Long Bones. New York, NY: Springer-Verlag; 1990
3 Browner BD. Skeletal Trauma: Fractures, Dislocations, Ligamentous Injuries. Philadelphia, PA: Saunders; 1992
4 Cooney WP. Fractures of the distal radius. A modern treatment-based classification. Orthop Clin North Am 1993;24(2): 211–216
5 Fernández DL. Fractures of the distal radius: operative treatment. Instr Course Lect 1993;42:73–88
6 Medoff RJ. Essential radiographic evaluation for distal radius fractures. Hand Clin 2005;21(3):279–288
7 Melone CP Jr. Distal radius fractures: patterns of articular fragmentation. Orthop Clin North Am 1993;24(2):239–253
8 Guitton TG, van der Werf HJ, Ring D. Quantitative measurements of the volume and surface area of the radial head. J Hand Surg Am 2010;35(3):457–463
9 Guitton TG, van der Werf HJ, Ring D. Quantitative three-dimensional computed tomography measurement of radial head fractures. J Shoulder Elbow Surg 2010;19(7):973–977
10 Teunis T, Bosma NH, Lubberts B, Ter Meulen DP, Ring D. MM Q3DCT radius. Available at: http://youtu.be/M0niRAoZ2xw. Accessed March 25, 2014
11 McCallister WV, Smith JM, Knight J, Trumble TE. A cadaver model to evaluate the accuracy and reproducibility of plain radiograph step and gap measurements for intra-articular fracture of the distal radius. J Hand Surg Am 2004;29(5): 841–847
12 Berger RA. The ligaments of the wrist. A current overview of anatomy with considerations of their potential functions. Hand Clin 1997;13(1):63–82
13 Zumstein MA, Hasan AP, McGuire DT, Eng K, Bain GI. Distal radius attachments of the radiocarpal ligaments: an anatomical study. J Wrist Surg 2013;2(4):346–350
14 Melone CP Jr. Open treatment for displaced articular fractures of the distal radius. Clin Orthop Relat Res 1986;(202):103–111
15 Mandziak DG, Watts AC, Bain GI. Ligament contribution to patterns of articular fractures of the distal radius. J Hand Surg Am 2011;36(10):1621–1625
16 Rikli DA, Honigmann P, Babst R, Cristalli A, Morlock MM, Mittlmeier T. Intra-articular pressure measurement in the radioulnocarpal joint using a novel sensor: in vitro and in vivo results. J Hand Surg Am 2007;32(1):67–75
17 Catalano LW III, Cole RJ, Gelberman RH, Evanoff BA, Gilula LA, Borrelli J Jr. Displaced intra-articular fractures of the distal aspect of the radius. Long-term results in young adults after open reduction and internal fixation. J Bone Joint Surg Am 1997; 79(9):1290–1302
18 Fritscher K, Karasev P, Pieper S, Kikinis R. (2014) Documentation/4.3/Extensions/VirtualFractureReconstruction. 3D Slicer. Available at: https://www.slicer.org/slicerWiki/index.php/Documentation/4.3/Extensions/VirtualFractureReconstruction. Accessed March 25, 2014